Front. Earth Sci. 2022, 16(4): 916–933
https://doi.org/10.1007/s11707-022-0969-2

RESEARCH ARTICLE

Fractal characterization of pore structure and its influence on CH_4 adsorption and seepage capacity of low-rank coals

Guangyuan MU[1], Haihai HOU[2], Jiaqiang ZHANG[3], Yue TANG[3], Ya-nan LI[1], Bin SUN[4], Yong LI[1], Tim JONES[5], Yuan YUAN[3], Longyi SHAO (✉)[1]

1 State Key Laboratory of Coal Resources and Safe Mining and College of Geoscience and Surveying Engineering, China University of Mining and Technology, Beijing 100083, China
2 College of Mining, Liaoning Technical University, Fuxin 123000, China
3 Oil & Gas Resource Survey Center, China Geological Survey, Ministry of Land and Resource, Beijing 100029, China
4 Department of Coalbed Methane, Research Institute of Petroleum Exploration and Development, PetroChina, Beijing 100083, China
5 School of Earth and Environmental Sciences, Cardiff University, Cardiff CF103YE, UK

Abstract The pore structures of coal can directly affect the adsorption and seepage capacity of coalbed methane (CBM), which therefore is an important influence on CBM exploration and development. In this study, the pore structures of low-rank coals from the Middle Jurassic Xishanyao Formation in the southern Junggar Basin were analyzed, and the fractal dimensions (D_1, D_2, D_3 and D_4 corresponding to pore sizes of 0–5 nm, 5–100 nm, 100–1000 nm and 1000–20000 nm, respectively) were calculated to quantitatively describe these coal pore structures. The results show that Xishanyao coal is characterized by open pore morphology, good pore connectivity and well-developed seepage pores and microfractures, which is beneficial to CBM seepage. The D_1 and D_2 can be used to characterize the pore surface and structure of adsorption pores respectively. The D_3 and D_4 can be used to represent the pore structure of seepage pores. Compared with adsorption pores, the structure of seepage pores is more affected by the change of coal rank. The D_1 is better than D_2 in characterizing the methane adsorption capacity. When $D_1 > 2.2$, D_1 is positively correlated with Langmuir volume (V_L) and negatively correlated with Langmuir pressure (P_L), while D_2 shows a weak opposite trend. The coals with the higher D_1 and lower D_2 are associated with a higher V_L, indicating the coal reservoir with more complex pore surfaces and simpler pore structures has stronger methane adsorption capacity. D_4 is better than D_3 in characterizing the methane seepage capacity. The porosity and permeability of coal reservoirs increase with the increase of D_4, while D_3 displays an opposite trend, which is mainly related to the well-developed microfractures. The well-developed fracture system enhances the seepage capacity of the Xishanyao coal reservoir. This study reveals the fractal characteristics of pore structure and its significant influence on adsorption and seepage capacity of low-rank coal.

Keywords southern Junggar Basin, Middle Jurassic, low-rank coal, coalbed methane, pore structure, fractal dimensions

Received July 19, 2021; accepted December 31, 2021

E-mail: ShaoL@cumtb.edu.cn

1 Introduction

Coal is a complex porous material formed by lengthy and different geological processes. Methane is mainly stored in coal pores by means of physical adsorption. As an important unconventional natural gas resource, coalbed methane (CBM) has attracted worldwide attention. China has realized the commercial exploitation of CBM in the Ordos and Qinshui Basins, but the production of CBM is mainly in the medium-high rank coal (Tao et al., 2014; Shao et al., 2015; Li et al., 2017). The low-rank coals have proved to be of great potential as the major coalbed methane reservoirs in the United States (Ayers, 2002; Flores et al., 2008; Qin et al., 2018). In China, very abundant low-rank coals are developed in the Mesozoic and Cenozoic coal basins (Cheng et al., 2016), and the CBM resources in these low-rank coals should be properly investigated. In recent years, the exploration of low-rank CBM has been carried out in many areas in China, among which exploration successes have been made in the Jiergalangtu Sag of Erlian Basin and the southern Junggar Basin (Li et al., 2016b; Sun et al., 2017). This indicates that low-rank CBM has a good

development potential, requiring the study of reservoir characteristics. The southern Junggar Basin is one of the key areas for low-rank CBM exploration in China, and its rich CBM resources have received extensive attention in recent years. Previous investigations in the study area primarily focused on the CBM enrichment model and resource potential evaluation, but the research on the physical properties of coal reservoirs was insufficient (Fu et al., 2016b, 2017b; Hou et al., 2021). The productivity and recovery efficiency of methane are significantly affected by the pore and fracture system of coal reservoirs (Zhou et al., 2018). Furthermore, in-depth research on the pore structure and its effect on adsorption and seepage of coal reservoirs in the southern Junggar Basin will contribute to future CBM exploration and development.

Coal pore structure, consisting of many components such as pore type, pore shape, pore volume, pore connectivity and pore size distribution (PSD), plays an important role in CBM enrichment. The pore structure, controlled by coalification, composition and macerals, can directly affect the adsorption and migration of CBM (Yao et al., 2008; Cai et al., 2013; Jiang et al., 2016; Mendhe et al., 2017). Therefore, the study of the pore structure of coal plays an important role in the exploration and development of coalbed methane. Coal pores can be subdivided into different types according to their geometry, connectivity and size. Based on their geometry, coal pores can be subdivided into cylindrical, conical, slit and ink-bottle. Based on their connectivity, the pores can be subdivided into closed, open, semi-open and cross-linked pores (Giesche, 2006; Wang et al., 2014; Nie et al., 2015). Based on their sizes, coal pores can be subdivided into micropores (diameter < 10nm), transition pores (10−100 nm), mesopores (100−1000 nm), and macropores (diameter > 1000 nm) (Hodot, 1966). Micropores and transition pores are also called adsorption pores, while mesopores and macropores are called seepage pores (Yao et al., 2008, 2009; Heriawan and Koike, 2015; Hou et al., 2017). Currently, there are many techniques available to characterize coal pore structures, such as CO_2 adsorption, low-temperature nitrogen adsorption (LTNA), mercury intrusion porosimetry (MIP), nuclear magnetic resonance (NMR) and scanning electron microscopy (SEM). LTNA and MIP are the two most commonly used methods, but both have limitations in the characterization of coal pore structures (Yao et al., 2008, 2009; Wang et al., 2020). LTNA can only obtain information about adsorption pores. MIP can damage the sample which results in reduction of the measured macropores due to the injection of high pressure mercury (Rodrigues and Lemos de Sousa, 2002; Mahamud and Novo, 2008; Yao and Liu, 2012; Wang et al., 2020). NMR is a non-destructive method to characterize coal properties such as porosity, permeability, pore connectivity, and pore size distribution (Yao et al., 2010; Sun et al., 2018). SEM can provide imagery of coal samples to qualitatively study the shape and size of coal pores (Li et al., 2016a; Hou et al., 2020a; Mou et al., 2021). In spite of the shortcomings of the individual methods, a combination of LTNA, MIP, NMR and SEM can effectively characterize the pore structures of coal, and LTNA and MIP can be further combined to characterize the specific PSD features (Fu et al., 2017a; Zhao et al., 2019).

After the fractal concept was proposed by Mandelbrot (1975), fractal analysis has been often used to quantitatively characterize the properties of porous reservoir rocks. Fractal theory provides a new approach for the study of coal pore structures and can effectively characterize the structural characteristics and heterogeneity of coal pores. Many researchers have made advances in the study of coal pore fractals, and published fractal models and their corresponding calculated fractal dimensions formulae of pore structures (Fu et al., 2001; Neimark, 1990; Yao et al., 2008, 2009). Previous studies have focused on the fractal characterization of coal pores within a specific pore size range, and only a few studies have focused on the fractal features of full-scale pores; especially low-rank coals (Fu et al., 2017a; Yao et al., 2008, 2009; Zhao et al., 2019). The different sizes of pores can affect the accumulation and development of coalbed methane; adsorption pores provide storage space for methane adsorption, and seepage pores provide channels for methane migration. Therefore, the fractal characterization of the pore structures in coal are of great significance in the exploration and development of coalbed methane.

In this study, the fractal dimensions were calculated based on LTNA and MIP data from coal samples, and the pore structures of coal were characterized. D_1 and D_2 were used to characterize the fractal characteristics of adsorption pores, while D_3 and D_4 were used to characterize the fractal characteristics of seepage pores. The influence of coal rank, composition, macerals, and pore structure on fractal dimension are discussed. Furthermore, the use of fractal dimensions to assess the adsorption capacity and seepage capacity of low-rank coal reservoirs was considered. This study will enhance our knowledge of pore structure systems in low rank coal and provide guidance in the future exploration and development of CBM.

2 Geological setting

The Junggar Basin, located in the southern part of the Siberian Plate and the eastern extension of the Kazakhstan Plate, is a giant intracontinental basin which underwent Hercynian, Indosinian, Yanshanian, and Himalayan multi-stage tectonic events from the late Palaeozoic to Quaternary (Chen and Arakawa, 2005; Ma et al., 2015; Shen et al., 2015; Tang et al., 2015; Fang et al., 2016). The southern Junggar Basin lies within the

piedmont thrust belt of the northern Tianshan Mountains (Fig. 1(a)). Structurally, the southern Junggar Basin can be divided into five secondary structural units from west to east: Sikeshu Sag, Qigu fault-fold belt, Huomatu anticlinal zone, Huan anticlinal zone, and Fukang fault zone (Fu et al., 2017b). The study area is located in the central part of the southern Junggar Basin where anticlines, synclines and monoclines are developed (Figs. 1(a) and 1(b)), and its tectonic evolution is controlled by the Qigu fault-fold belt.

The Jurassic strata in the southern Junggar Basin are composed of the Badaowan and Sangonghe Formations of the Lower Jurassic; Xishanyao and Toutunhe Formations of the Middle Jurassic; Qigu and Kalaza Formations of the Upper Jurassic (Ashraf et al., 2010). The main coal-bearing strata found in the study area are the Badaowan Formation and the Xishanyao Formation. The coal seams of the Badaowan Formation in the central part of the southern Junggar Basin are very thin due to tectonic uplift and an alluvial fan depositional environment (Fu et al., 2016b; Li et al., 2018). Therefore, the Xishanyao Formation was selected as the target for CBM exploration and development because of the large thickness and suitable burial depth of the coal seams. Lithologically, the Xishanyao Formation is composed of conglomerates, sandstones, siltstones, mudstones, and coals, and this formation can be subdivided into the bottom thick coal seam member, the thin middle coal seam member, and the top member without coal (Fig. 1(c)). Previous studies have showed that the sediments of the Xishanyao Formation were mainly developed in fluvial, deltaic and lacustrine sedimentary environments (Shao et al. 2003; Li et al. 2018; Hou et al. 2020b, 2021).

3 Sampling, experimental methods and fractal theory

3.1 Sampling and experimental methods

A total of 18 coal samples were collected from 6 different sites in the southern Junggar Basin, all of which were from the Middle Jurassic Xishanyao Formation (Fig. 1(b)). The samples were carefully packed to preserve their initial form and structure, and then immediately sent to the experimental institutions for testing.

The experiments performed in this study included identifying the coal lithotype, maximum vitrinite reflectance ($R_{o,max}$, %), coal proximate analysis, coal macerals, LTNA, MIP, SEM, NMR, and methane isothermal adsorption experiments. The coal lithotypes are classified according to the Chinese National Standard GB/T 18023-2000. A Leitz MPV-3 photometer was used to determine $R_{o,max}$ and coal macerals according to the Chinese National Standards GB/T 6948-1998 and GB/T 8899-1998, respectively. The proximate analysis test was conducted following the Chinese National Standard GB/T 30732-2014. The LTNA test was conducted using a Quantachrome NOVA2000e analyzer following the Chinese National Petroleum Industry Standard SY/T

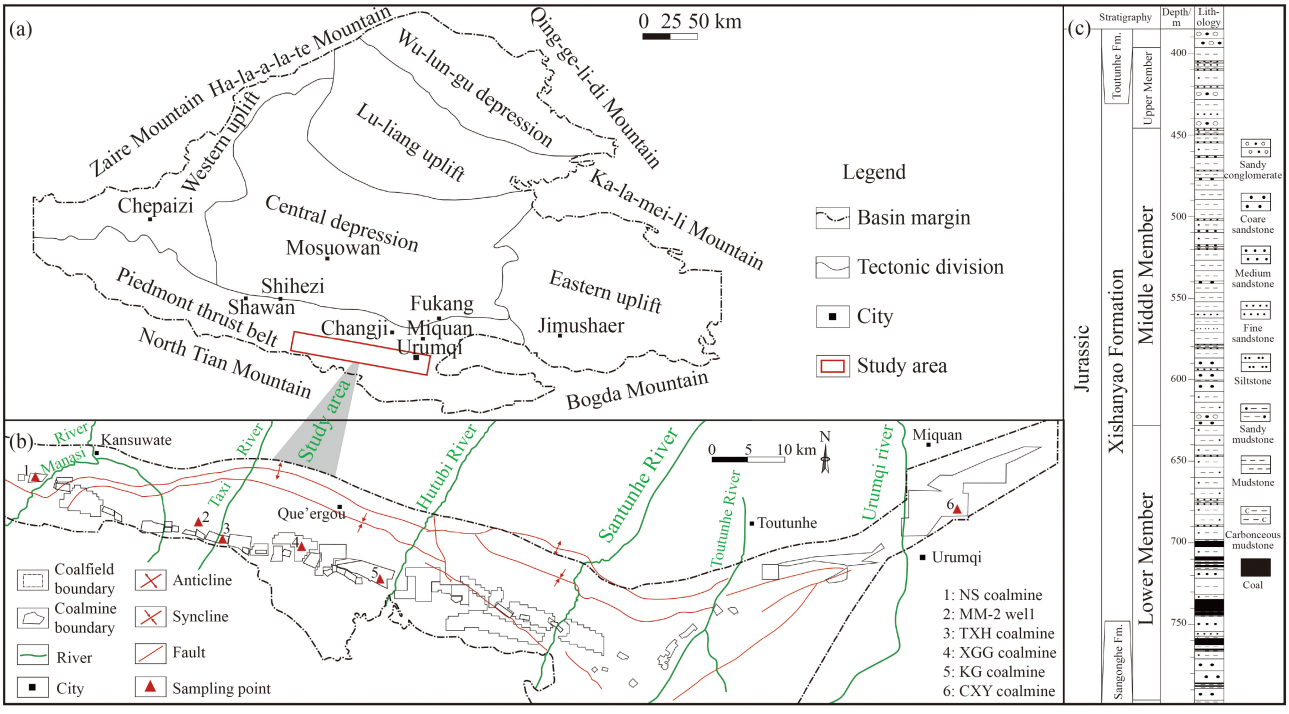

Fig. 1 (a) Position of the study area in Junggar Basin (modified from Fu et al., 2016b). (b) Distribution of sampling points in the southern Junggar Basin. (c) Stratigraphic column for the coal-bearing strata in southern Junggar Basin.

6154-1995. The specific surface area and volume of adsorption pores were calculated using the Brunauer-Emmett-Teller (BET) model and the Barrett-Joyner-Halenda (BJH) model, respectively (Brunauer et al., 1938; Barrett et al., 1951). The MIP was performed using a Quantachrome PoreMaster 33 instrument following the Chinese National Petroleum Industry Standard SY/T 5346-2005. The pore characteristics of the coal samples were observed under a JSM-7500F field emission scanning electron microscope (15KV). NMR tests were performed using a MicroMR12-025V analyzer. The methane isothermal adsorption experiment was conducted according to the Chinese National Standard GB/T 19560-2008, using an IS-100 high-pressure isothermal adsorption device. The test temperature and maximum adsorption pressure were 30°C and 10 MPa, respectively.

3.2 Fractal theory of adsorption pores

The Frenkel-Halsey-Hill (FHH) model is often used to study the fractal characteristics of adsorption pores based on nitrogen adsorption data, and its reliability and quality has been confirmed by previous researchers (Pfeifer et al., 1989; Yao et al., 2008; Zhao et al., 2019). The FHH model can be described as follows:

$$\ln V = C + A\left[\ln\left[\ln\frac{P_0}{P}\right]\right], \tag{1}$$

where V is the volume of gas adsorbed at equilibrium pressure P, cm^3/g; P_0 is the saturation pressure of gas adsorption, MPa; P is the equilibrium pressure, MPa; A is the slope of double logarithm curve of ln$V$ vs. ln(ln(P_0/P)); C is a constant.

The fractal dimension D can be obtained by slope A, and corresponding formulas should be used for calculation at different adsorption stages. When the early stage of adsorption is controlled by van der Waals forces, D should be calculated by Eq. (2):

$$D = 3A + 3. \tag{2}$$

However, when the gas adsorption process is dominated by capillary condensation, Eq. (3) should be used to calculate the fractal dimension D:

$$D = A + 3. \tag{3}$$

3.3 Fractal theory of seepage pores

The fractal dimension of seepage pores can be obtained by using different calculation models (including geometric models and thermodynamic models) according to MIP data (Pfeifer and Avnir, 1983; Friesen and Mikula, 1987; Mahamud, 2006; Yao et al., 2009). In this study, a widely used geometric model is used to calculate the fractal dimension of coal seepage pores. The model is described as follows:

$$\ln\left[\frac{\mathrm{d}V}{\mathrm{d}P}\right] = A\ln P, \tag{4}$$

where P is the mercury injection pressure, MPa; V is the cumulative injection volume at a given pressure P, cm^3/g; A is the slope of double logarithm curve of ln$P$ vs. ln(dV/dP).

The fractal dimension D based on MIP data can be calculated by Eq. (5):

$$D = A + 4. \tag{5}$$

4 Results

4.1 Petrology, proximate analysis, and methane isothermal adsorption test

Several conventional tests were carried out on the coal samples, including coal lithotype, maceral compositions, maximum vitrinite reflectance ($R_{o,max}$), proximate analysis and the CH_4 isothermal adsorption test (Table 1). The Xishanyao coal samples are dominated by semi-bright coals, followed by bright coals and semi-dull coals. In terms of Langmuir volume, bright coals have the best methane adsorption capacity, followed by semi-bright coals and semi-dull coals. The $R_{o,max}$ values of the low-rank coal samples vary from 0.57% to 0.72%, with an average of 0.63%. Based on the air-dried data, moisture content ranges from 1.75% to 4.74% (avg. 3.04%), the ash yield and the volatile matter content ranges from 2.57% to 26.45% (avg. 8.91%) and 27.91% to 38.32% (avg. 33.77%), respectively. The range of fixed carbon content is 43.60%−65.04%, with an average of 55.42%. The proximate analysis results show that the Xishanyao coal in the southern Junggar Basin is characterized by a low moisture content, a low ash yield and a high volatile matter content. The vitrinite, inertinite, and liptinite contents are 45.61%−90.32% (avg. 66.10%), 4.07%−48.92% (avg. 27.70%) and 0.58%−11.94% (avg. 4.50%), respectively. The vitrinite content of MM2-4 sample is abnormally high, with a value of 90.32%.

The methane isothermal adsorption results of the Xishanyao coal show that the Langmuir volume (V_L) is 9.76−18.16 m^3/t, with an average of 12.76 m^3/t, and the Langmuir pressure (P_L) is 3.79−5.82 MPa, with an average of 4.79 MPa. The results indicate that the Xishanyao coal in the southern Junggar Basin has medium methane adsorption capacity, but the low P_L is not favorable for methane desorption, which increases the difficulty of CBM development.

4.2 Low-temperature nitrogen adsorption

The LTNA experiments are often used to characterize the pore size distribution and pore morphology of coal

Table 1 Results of lithotype, maximum vitrinite reflectance, proximate analysis, maceral and CH_4 isothermal adsorption of the coal samples from southern Junggar Basin

Sample No.	Coal lithotype	$R_{o,max}$/%	Proximate analysis/wt%				Coal macerals/%			CH_4 isothermal adsorption	
			M_{ad}	A_{ad}	V_{ad}	FC_{ad}	V	I	L	V_L/($m^3 \cdot t^{-1}$)	P_L /MPa
NS-1	semi-bright	0.62	4.74	13.87	31.10	50.29	45.61	48.92	5.47	9.76	5.05
NS-2	semi-bright	0.59	4.54	10.92	32.98	51.56	54.61	38.32	7.07	n	n
MM2-1	bright	0.58	2.29	16.38	37.73	43.60	77.23	7.67	10.89	n	n
MM2-2	bright	0.62	2.26	11.69	-	-	74.00	11.48	10.54	n	n
MM2-3	semi-bright	0.72	1.75	26.45	-	-	81.16	7.73	0.97	n	n
MM2-4	semi-bright	0.64	2.08	13.69	37.73	46.50	90.32	4.15	4.61	n	n
MM2-5	bright	0.65	2.27	8.07	38.00	51.66	89.43	4.07	4.88	n	n
MM2-6	semi-dull	0.66	2.10	7.00	34.15	56.75	78.28	17.21	4.51	n	n
MM2-7	semi-bright	0.65	1.84	12.63	38.32	47.21	79.10	8.96	11.94	n	n
TX-1	bright	0.68	3.59	6.94	30.02	59.45	56.93	40.67	2.40	15.43	5.11
TX-2	semi-bright	0.69	3.02	4.03	27.91	65.04	59.60	37.80	2.60	n	n
XGG-1	bright	0.65	3.82	3.97	30.52	61.69	62.50	34.05	3.45	n	n
KG-1-1	semi-dull	0.59	3.35	5.74	35.23	55.68	58.85	36.21	3.29	9.85	4.12
KG-1-2	semi-bright	0.64	3.49	3.03	34.19	59.29	53.38	42.62	1.48	11.22	4.74
KG-1-3	semi-bright	0.64	3.79	2.57	32.62	61.02	49.80	44.80	2.80	12.94	5.11
KG-1-4	semi-bright	0.60	3.69	2.80	32.95	60.56	59.50	38.39	0.58	14.12	5.82
KG-1-5	semi-dull	0.58	3.78	5.48	32.79	57.95	53.80	43.41	1.30	10.62	4.57
CXY-2	bright	0.57	2.24	5.08	34.15	58.53	65.62	32.08	2.31	18.16	3.79

Notes: $R_{o,max}$, maximum vitrinite reflectance; M_{ad}, moisture content, air-dried basis; A_{ad}, ash yield, air-dried basis; V_{ad}, volatile content, air-dried basis; FC_{ad}, fixed carbon content, air-dried basis; V, vitrinite; I, inertinite; L, liptinite; V_L, Langmuir volume; P_L, Langmuir pressure; -, no data; n, not analyzed.

(Hassan, 2012; Zhang et al., 2014; Pan et al., 2016; Zhu et al., 2016; Hou et al., 2018, 2020a). As shown in Table 2, the average pore diameter of coal samples ranges from 6.32 to 15.86 nm, with an average of 8.77 nm. The BET specific surface area varies from 0.116 to 2.287 m^2/g, with an average of 1.006 m^2/g. The BJH pore volume ranged from 0.365 to 4.339 × 10^{-3} cm^3/g, with an average of 1.913 × $10^{-3}$$cm^3/g$. As shown in Figs. 2(b) and 2(c), the BET specific surface area is dominated by micropores, while the BJH pore volume is mainly provided by micropores and transition pores. Based on the LTNA results, the pore volume of coal is dominated by micropores, accounting for 27.49%–79.77% (avg. 53.48%), transition pores and mesopores accounting for 17.92%–58.20% (avg. 39.42%) and 1.10%–14.31% (avg. 7.11%), respectively. The LTNA experiment is more sensitive to the micropores and transition pores, but mesopores and macropores larger than 200 nm are problematic to measure.

Based on the LTNA results, the typical adsorption/desorption curves, BJH pore volume distribution and BET specific surface area distribution of coal samples from the Xishanyao Formation were obtained (Fig. 2). According to the classification published by the International Union of Pure and Applied Chemistry (IUPAC) (Thommes et al., 2015), the Xishanyao coal consist of type II and type IV physisorption isotherms and H2 and H3 hysteresis loops. Based on the hysteresis loop classification, nitrogen adsorption/desorption curves are divided into three types: Type A, Type B and Type C (Table 2, Fig. 2). For the Type A coal, the specific surface area and total pore volume are relatively large and showing the type II physisorption isotherm. The desorption curve decreases sharply at the relative pressure of 0.5, which conforms to the H2 hysteresis loop and corresponds to ink-bottle shaped pores (Fig. 2(a-1)). Pore volume is dominated by micropores, with few transition pores and mesopores, and pore specific surface area is only provided by micropores (Figs. 2(b-1) and 2(c-1)). Ink-bottle shaped pores and extremely high micropore content are favorable for gas adsorption and enrichment, but not for desorption and seepage. Type B coal has type II physisorption isotherms but the H3 type hysteresis loop. The smaller hysteresis loops represent open pores at both ends (e.g., cylindrical pores or parallel plate-like pores), which is conducive to gas seepage. Pore volume is dominated by micropores, followed by transition pores and mesopores, and pore specific surface area is mainly provided by micropores (Figs. 2(b-2) and 2(c-2)). With Type C coal, the specific surface area and total pore volume are small. Physisorption isotherms begin to rise sharply after the relative pressure reached 0.9, which belongs to type IV. The hysteresis loop is not obvious, indicating closed pores at one end, such as plate-like or slit-like pores. The total pore volume and specific surface area are mainly provided by micropores and transition

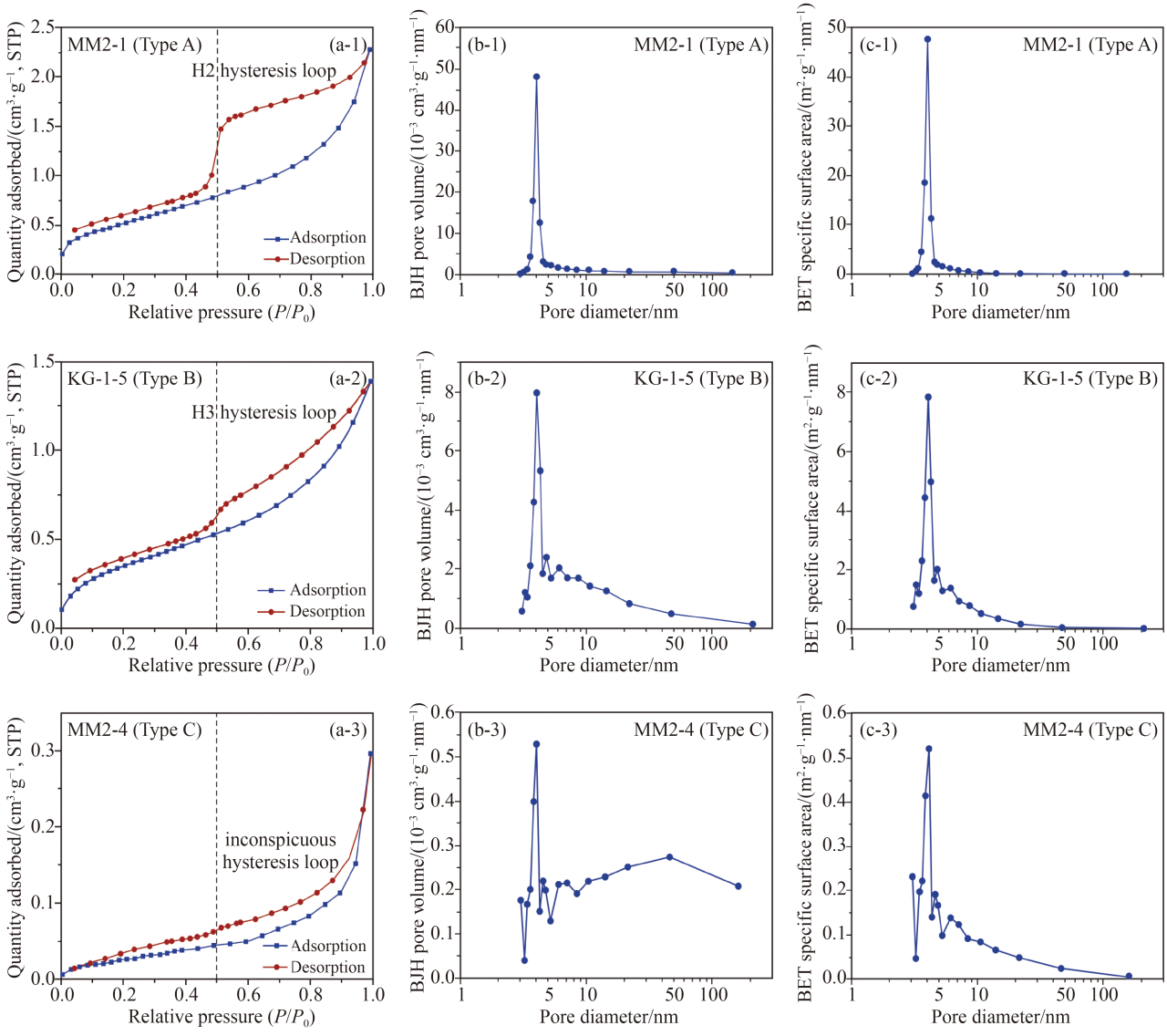

Fig. 2 Three types of nitrogen adsorption/desorption results and pore size distribution based on LTNA for typical Xishanyao coal samples. (a) Nitrogen adsorption/desorption curves. (b) BJH pore volume distribution. (c) BET specific surface area distribution.

pores (Figs. 2(b-3) and 2(c-3)). Type C coal is favorable for gas seepage and not conducive to gas adsorption. As shown in Table 2, the adsorption/desorption curves are dominated by Type B and Type C, indicating that low-rank coal from the Xishanyao Formation is conducive to CBM seepage, but not to adsorption.

4.3 Mercury intrusion porosimetry

The MIP results of the coal samples include helium porosity, air permeability, average pore throat diameter, average pore diameter, total mercury intrusion volume, mercury saturation and extrusion efficiency (Table 3). The porosity ranges from 3.17% to 7.55%, with an average of 5.04%. The permeability ranges from 0.001 to 151.660 mD, with an average of 16.187 mD. The unusually high permeability of individual samples may be caused by the high content of microfractures. The average pore throat diameter ranges from 18 to 70 nm (avg. 29.33 nm), and the average pore diameter ranged from 24 to 1992 nm (avg. 590 nm). The total mercury intrusion volume varies from 0.31 to 0.77 mL, with an average of 0.53 mL. The maximum mercury saturation is 85.54%–94.45%, with an average of 91.41%. The extrusion efficiency ranges from 48.85 to 86.23%, with an average of 70.74%. The PSD based on MIP data shows that the coal pores are dominated by transition pores (37.43%–63.04%, avg. 52.27%), followed by micropores (10.53%–24.16%, avg. 18.37%), mesopores (8.67%–27.75%, avg. 15.19%), and macropores (6.65%–32.22%, avg. 14.17%). Generally, the seepage pores of low-rank coal are more developed. It is noted that the high adsorption pore content in the experimental results may be due to the destruction of the coal matrix by high-pressure mercury injection.

Table 2 Results of low-pressure nitrogen adsorption, fractal dimension and loop type of coal samples from southern Junggar Basin

Sample No.	PD_1 /nm	S_{BET} /($m^2 \cdot g^{-1}$)	V_{BJH} /($10^{-3} cm^3 \cdot g^{-1}$)	Pore content /volume (%)			P/P_0: 0−0.5 (0−5 nm)			P/P_0: 0.5−1 (5−100 nm)			Loop type
				V_{N1}	V_{N2}	V_{N3}	A_1	$D_1 = 3 + A_1$	R^2	A_2	$D_2 = 3 + A_2$	R^2	
NS-1	7.81	0.756	1.477	43.96	49.83	6.20	−0.8435	2.1565	0.9745	−0.2478	2.7522	0.9539	C
NS-2	10.49	0.731	1.917	43.03	45.76	11.21	−0.8133	2.1867	0.9680	−0.2935	2.7065	0.9468	C
MM2-1	7.24	1.922	3.477	79.77	17.92	2.31	−0.5951	2.4049	0.9861	−0.2419	2.7581	0.9490	A
MM2-2	13.04	0.283	0.922	50.85	40.23	8.92	−0.7480	2.2520	0.9839	−0.3572	2.6428	0.9784	B
MM2-3	11.58	0.264	0.763	41.22	46.67	12.11	−0.8443	2.1557	0.9727	−0.3227	2.6773	0.9544	C
MM2-4	15.86	0.116	0.461	27.49	58.20	14.31	−0.8758	2.1242	0.9801	−0.4224	2.5776	0.9775	C
MM2-5	7.72	0.283	0.546	60.02	33.25	6.73	−1.0758	1.9242	0.9712	−0.2437	2.7563	0.9195	B
MM2-6	9.44	0.284	0.671	39.86	50.97	9.17	−0.8195	2.1805	0.9703	−0.2800	2.7200	0.9479	C
MM2-7	8.24	0.177	0.365	45.81	42.56	11.63	−1.0417	1.9583	0.9782	−0.2445	2.7555	0.9318	C
TX-1	8.46	1.417	2.995	51.62	40.36	8.02	−0.7038	2.2962	0.9701	−0.2571	2.7429	0.9297	B
TX-2	7.59	2.287	4.339	52.64	39.82	7.54	−0.6647	2.3353	0.9640	−0.2332	2.7668	0.9301	B
XGG-1	6.32	1.811	2.860	69.79	29.11	1.10	−0.7029	2.2971	0.9604	−0.2036	2.7964	0.8749	B
KG-1-1	7.59	1.114	2.113	56.55	39.84	3.61	−0.7110	2.2890	0.9647	−0.2454	2.7546	0.9121	B
KG-1-2	7.13	1.399	2.493	63.11	34.15	2.74	−0.7068	2.2932	0.9567	−0.2370	2.7630	0.8930	B
KG-1-3	6.85	1.950	3.340	64.96	30.82	4.22	−0.7161	2.2839	0.9630	−0.1824	2.8176	0.8258	B
KG-1-4	6.80	1.665	2.829	66.13	31.58	2.29	−0.7587	2.2413	0.9550	−0.2218	2.7782	0.8704	B
KG-1-5	6.41	1.342	2.151	64.25	32.28	3.48	−0.7259	2.2741	0.9554	−0.1978	2.8022	0.8681	B
CXY-2	9.26	0.305	0.705	41.50	46.15	12.35	−0.8796	2.1204	0.9787	−0.2647	2.7353	0.9256	C

Notes: PD_1, average pore diameter; S_{BET}, BET special surface area; V_{BJH}, BJH total pore volume;V_{N1}, content of micropore (< 10 nm in diameter); V_{N2}, content of transition pore (10−100 nm in diameter); V_{N3}, content of mesopore (100−1000 nm in diameter); N, based on LTNA; D_1, fractal dimension with pore diameter ranging from 0 to 5 nm; D_2, fractal dimension with pore diameter ranging from 5 to 100 nm.

Table 3 Results of mercury intrusion porosimetry, fractal dimension and curve type of coal samples from southern Junggar Basin

Sample No.	Φ/%	K_{air}/mD	PTD/nm	PD_2/nm	V_{in}/mL	MMS/%	E_{ex}/%	Pore content/volume (%)				100−1000 nm		1000−20000 nm		Curve type
								V_{M1}	V_{M2}	V_{M3}	V_{M4}	D_3	R^2	D_4	R^2	
NS-1	7.55	2.193	70	1238	0.77	91.71	48.85	13.27	37.43	27.69	21.61	2.9333	0.9951	3.8779	0.1259	B
NS-2	5.43	151.660	24	1378	0.55	88.49	67.76	18.24	45.39	13.81	22.56	3.1496	0.9872	3.4407	0.7197	C
MM2-4	4.48	0.010	30	1992	0.43	90.92	64.69	16.69	41.62	9.47	32.22	3.1272	0.9298	3.4048	0.4309	D
TX-1	6.97	2.448	54	680	0.75	91.55	50.39	12.77	42.47	27.75	17.01	3.3120	0.9730	3.7063	0.7350	B
TX-2	5.59	0.181	32	266	0.63	93.95	58.34	16.11	51.54	23.05	9.31	3.4470	0.9791	3.6623	0.6047	B
XGG-1	4.77	0.051	20	666	0.45	90.21	77.89	21.83	53.59	9.83	14.76	3.5192	0.9297	3.5303	0.7076	A
KG-1-1	3.17	0.130	24	666	0.31	85.54	82.87	10.53	63.04	10.62	15.81	3.6084	0.8771	3.4573	0.6852	C
KG-1-2	4.34	1.080	20	48	0.50	94.45	73.77	20.33	58.33	14.18	7.16	3.5868	0.9790	3.3311	0.8567	A
KG-1-3	4.28	0.001	18	26	0.46	90.05	86.23	24.16	60.52	8.67	6.65	3.6904	0.7986	3.2492	0.7861	A
KG-1-4	4.31	0.005	18	24	0.49	93.07	82.48	23.79	56.57	11.08	8.56	3.8566	0.5926	3.4618	0.5742	A
KG-1-5	4.48	0.002	18	44	0.47	93.95	81.67	23.23	59.56	10.38	6.83	3.6208	0.6909	3.5492	0.8517	A
CXY-2	5.08	36.482	24	52	0.57	92.99	73.99	19.51	57.14	15.73	7.61	3.6773	0.8852	3.5471	0.6786	A

Notes: Φ, helium porosity; K_{air}, air permeability; PTD, average pore throat diameter; PD_2, average pore diameter; V_{in}, total mercury intrusion volume; MMS, maximum mercury saturation; E_{ex}, extrusion efficiency;V_{M1}, content of micropore (< 10 nm in diameter); V_{M2}, content of transition pore (10−100 nm in diameter); V_{M3}, content of mesopore (100−1000 nm in diameter); V_{M4}, content of macropore (> 1000 nm in diameter); M, based on MIP; D_3, fractal dimension with pore diameter ranging from 100 to 1000 nm; D_4, fractal dimension with pore diameter ranging from 1000 to 20000 nm.

Typical mercury intrusion/extrusion curves obtained by the MIP experiments are shown in Fig. 3. According to the maximum mercury saturation, extrusion efficiency and mercury injection volume in each pore size stage, the mercury intrusion/extrusion curves can be divided into four types: Type A, Type B, Type C, and Type D (Table 3, Fig. 3). For Type A, the maximum mercury saturation and extrusion efficiency of coal are high, which indicates

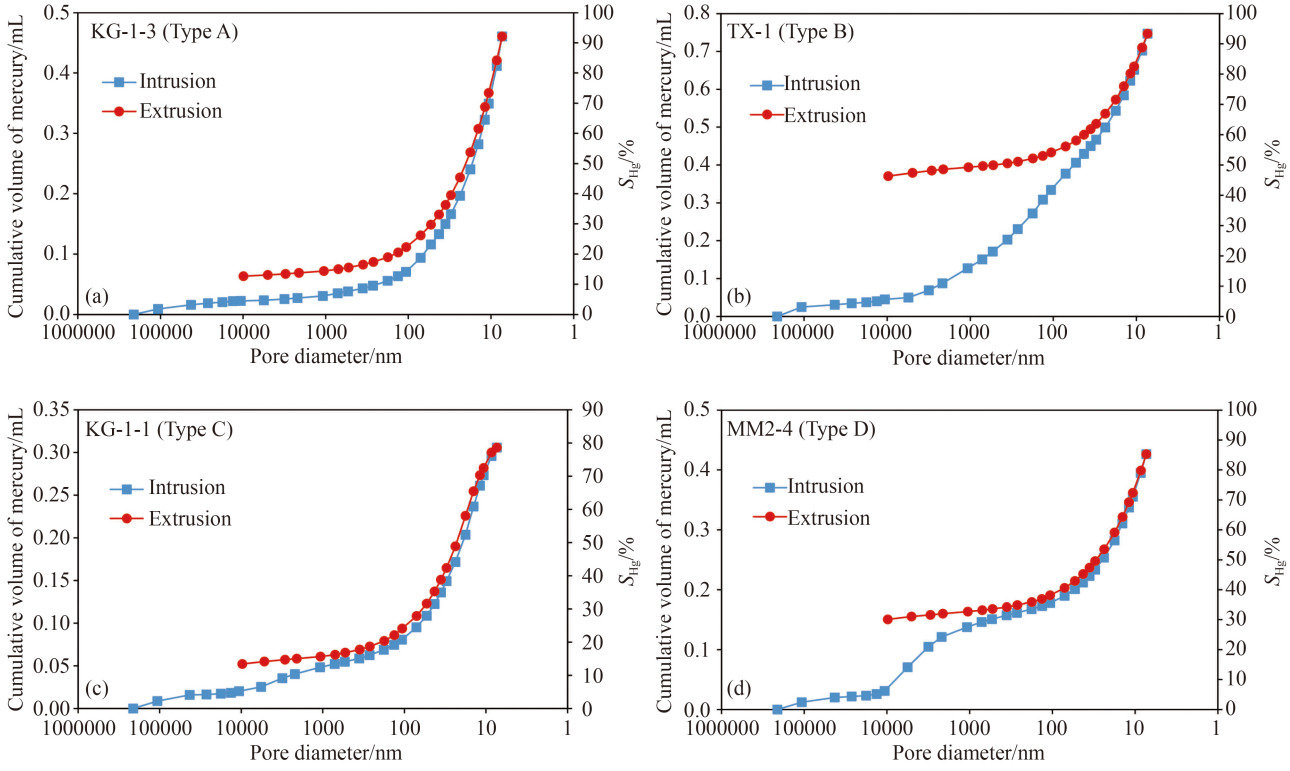

Fig. 3 Four types of mercury intrusion/extrusion curves based on MIP for typical Xishanyao coal samples from the southern Junggar Basin.

good pore connectivity. The mercury intrusion curve is divided into two stages, and the mercury intrusion volume is mainly provided by the transition pores (Fig. 3(a)). For Type B, the total mercury intrusion volume is the highest, and the maximum mercury saturation is like Type A, but the extrusion efficiency is low. The mercury intrusion curve is also divided into two stages, and the mercury intrusion volume is mainly provided by transition pores and mesopores (Fig. 3(b)). Type C coal is characterized by low maximum mercury saturation. The mercury intrusion curve is divided into three stages, with the mercury intrusion volume mainly corresponding to transition pores (Fig. 3(c)). Type D coal has a high maximum mercury saturation and moderate extrusion efficiency. The mercury intrusion curve is divided into four stages, and the mercury injection is mainly provided by transition pores and macropores (Fig. 3(d)). Type A accounts for the largest proportion of the coal samples, indicating that the Xishanyao coal has good pore connectivity, which is conducive to coalbed methane seepage and production.

4.4 Scanning electron microscopy

The LTNA and MIP methods can only be used to characterize the pore structures of coal within a certain pore size range, whereas SEM can be used to directly obtain structural features of the coal pore-fracture system. Therefore, the microstructure of pores, fractures, and macerals of the Xishanyao coal were observed separately by SEM. There are widely developed primary pores and sparse gas pores in fusinite (Fig. 4(a)). The shape of the gas pores is mainly circular or ellipse, with smooth edges, clear outline and no infilling, reflecting the original plant structure. Gas pores are direct evidence of coal gas production, and their appearance indicates that the Xishanyao low-rank coal has certain gas content. In the telocollinite, a series of gas pores are distributed in strips (Fig. 4(b)). There are sparse gas pores in the corpocollinite, with the primary pores developed between the corpocollinite bodies (Fig. 4(c)). There are numerous fractures developed in the vitrinite, including endogenous microfractures and exogenous structural fractures (Figs. 4(d) and 4(f)), which are conducive to coalbed methane seepage and development. The cells of some deformed fusinite are filled with clay minerals (Fig. 4(e)). Both structural fractures and fusinite deformation indicate that the Xishanyao coal has experienced tectonic geological stresses. From the SEM observation, it is concluded that the primary seepage pores and microfractures in Xishanyao coal are well developed.

4.5 Fractal dimension characteristics of the coal pores

4.5.1 Fractal dimensions of adsorption pores

Based on the LTNA data, the fractal dimensions are often used to quantitatively characterized the structure of adsorption pores (Yao et al., 2008; Zhao et al., 2019). To calculate the fractal dimension values, the double logarithmic diagrams of $\ln(P_0/P)$ and $\ln(V)$ were obtained based on LTNA experiments (Fig. 5). These plots are

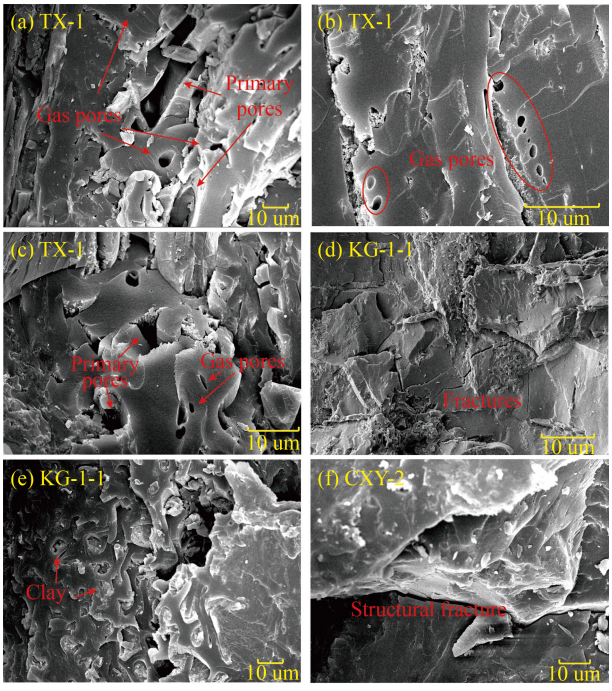

Fig. 4 SEM images show pore and maceral characteristics of typical coal samples. (a) widely developed primary pores and sparse gas pores in fusinite; (b) many gas pores were developed in telocollinite; (c) primary pores and gas pores in the corpocollinite; (d) microfractures were widely developed in vitrinite; (e) primary pores infilled with clay minerals in deformed fusinite; (f) structural fractures in the vitrinite.

divided into two distinct sections with $\ln(\ln(P_0/P)) = -0.5$ (corresponding $P/P_0 = 0.5$) as the cut-off point, and the aperture corresponding to the cut-off point is about 5 nm. A is the slope of the regression line and can be used to calculate the fractal dimension D. A_1 and A_2 were obtained in the range of $\ln(\ln(P_0/P)) < -0.5$ and $\ln(\ln(P_0/P)) > -0.5$, respectively. D_1 and D_2 represent the fractal dimension of the pore surfaces and structures, respectively, which has been confirmed by previous studies (Yao et al., 2008; Wang et al., 2015; Tao et al., 2018). It should be noted that there are two commonly used formulas to calculate fractal dimension D: "$3-(A+1)$" and "$A+3$". The latter can calculate more creditable fractal dimensions, while the former results are often less than 2, which deviates from the natural fractal dimension (2–3) (Yao et al., 2008; Li et al., 2016b; Fu et al., 2017a). Therefore, "$D=A+3$" was adopted in this study to calculate the fractal dimensions of coal, and the calculation results are shown in Table 2. D_1 ranges from 1.9242 to 2.4049, with an average of 2.2096. D_2 ranges from 2.5776 to 2.8176, with an average of 2.7391. The D_1 values of sample MM2-5 and MM2-7 are less than 2, deviating from the natural fractal dimension, which may be attributed to the low specific surface areas and surface roughness of coal pores. The abnormally high D_1 value of sample MM2-1 is due to the extremely high micropores content and very rough pore surfaces. D_1 and D_2 have a weak positive correlation (Fig. 6), which is also seen in previous study (Fu et al., 2017a).

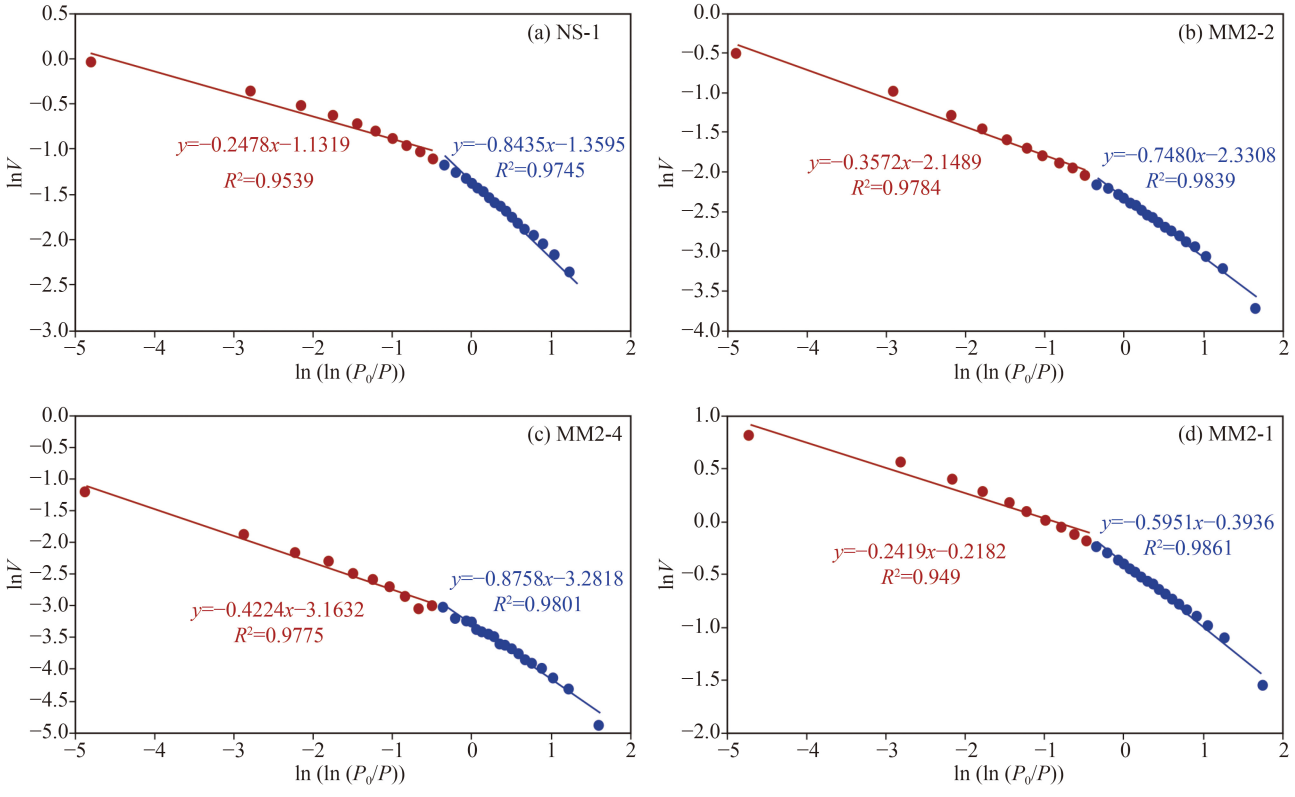

Fig. 5 Diagrams showing representative examples of the relationship between $\ln(\ln P_0/P)$ and $\ln V$ for typical low-rank coal samples.

4.5.2 Fractal dimensions of seepage pores

Based on the mercury injection volume and pressure obtained by the MIP experiments, the double logarithmic diagrams of ln$P$ and ln(dV/dP) were obtained (Fig. 7). As discussed above, the coal matrix compression starts when the pore diameter is 100 nm (corresponding pressure is 13 MPa), and the damage to the pore structures of the coal cannot be ignored. Therefore, only the MIP data with pore diameters greater than 100 nm can be used to study the fractal characteristics of low-rank coal, which is consistent with previous studies (Yao et al., 2009). The double logarithm relation has obvious segmental characteristics. The two sections of "d = 100−1000 nm" and "d = 1000−20000 nm" are fitted linearly, and the fractal dimensions D_3 and D_4 are calculated by Eqs. (3) and (4) (Fig. 7, Table 3). D_3 ranges from 2.9333 to 3.8566, with an average of 3.4607. D_4 ranges from 3.2492 to 3.8779, with an average of 3.5182. There is a weak negative correlation between D_3 and D_4 (Fig. 8). The D_3 and D_4 values of most coal samples are larger than 3, beyond the natural fractal dimension, which may be due to the abnormally high pore heterogeneity caused by the deformation of low-rank coal under externally derived stresses. This is consistent with the structural fractures observed by SEM in Fig. 4(f).

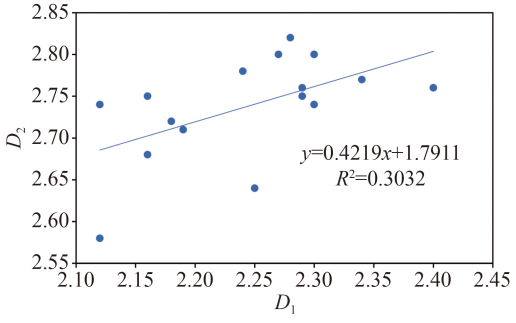

Fig. 6 Relationship between fractal dimensions D_1 and D_2.

5 Discussion

5.1 Comparison analysis by LTNA and MIP joint and NMR

Both LTNA and MIP can be used to determine the pore volumes and pore size distributions (PSD) of the coal. The LTNA is only suitable for adsorption pores, while both adsorption and seepage pores can be measured by MIP (Rodrigues and Lemos de Sousa, 2002; Hassan, 2012; Yao and Liu, 2012). However, the shielding effect of small pores on larger pores and the destruction of the coal matrix caused by the high pressure mercury injection will affect the accuracy of pore content measurements. (Mahamud and Novo, 2008; Yao and Liu, 2012). Therefore, the compression and damage to the coal matrix must be considered when analyzing the PSD of coal. The mercury intrusion curves of the coal samples are shown in Fig. 9, and there are obvious yielding points at 100 nm (corresponding to the pressure of 13 MPa). The cumulative mercury volume increases slowly when the pore diameter is > 100 nm but increases rapidly when the pore diameter is < 100 nm, indicating that the coal matrix compression occurs at this point, and the pore content less than 100 nm measured by MIP is not accurate. This further indicates that MIP is not suitable for the determination of the adsorption pore content of the coal.

NMR provides a non-destructive method to characterize coal properties such as porosity, permeability, pore connectivity and PSD (Yao et al., 2010; Sun et al., 2018). The coal samples were analyzed by NMR under saturated water, and the T_2 spectrum of most coal samples showed a single peak distribution, with the peak value biased toward the seepage pores and microfractures (Fig. 10(b)). To accurately characterize the PSD of the coal samples, the incremental pore volume measured by LTNA and MIP was connected at 100 nm, and the obtained PSD results were compared with those evaluated by NMR (Fig. 10). The results showed that the PSD evaluated by the combination of LTNA and MIP was in good agreement with those obtained by the NMR, indicating that this joint evaluation method was more accurate. The PSD results obtained by combining the two methods are

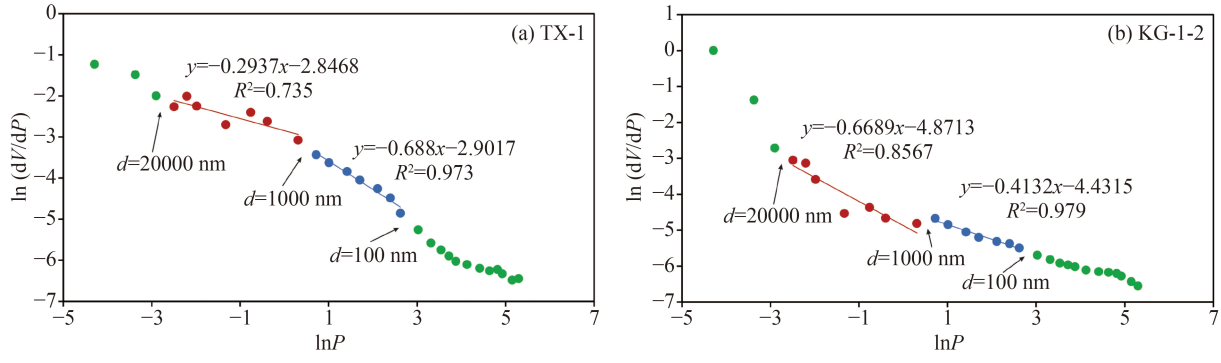

Fig. 7 Diagrams showing representative examples of the relationship between ln$P$ and ln(dV/dP) for typical low-rank coal samples.

shown in Table 4, the pores developed in Xishanyao low-rank coals are mainly mesopores (22.22%–63.63%, avg. 43.05%), macropores and microfractures (23.07%–75.34%, avg. 38.86%), while micropores (0.79%–24.23%, avg. 10.73%) and transition pores (1.65%–14.01%, avg. 7.36%) are poorly developed (Fig. 10(a)). Consequently, the Xishanyao coal pores are mainly seepage pores and microfractures, and the pore connectivity is good, which is conducive to the flow and development of CBM.

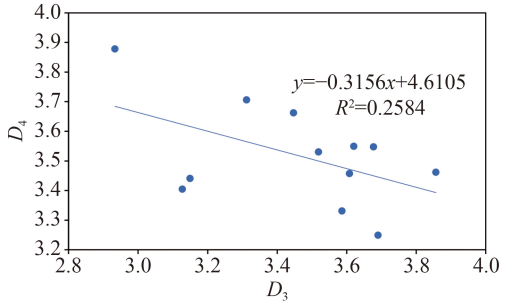

Fig. 8 Relationship between fractal dimensions D_3 and D_4.

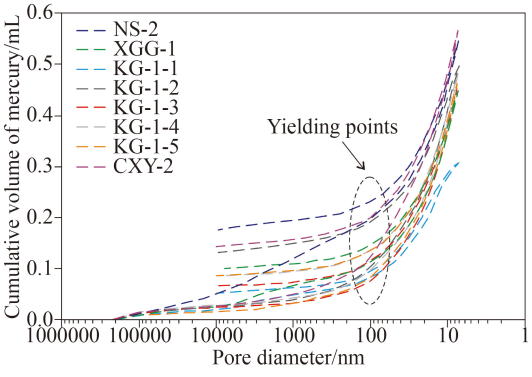

Fig. 9 Mercury intrusion/extrusion curves show coal matrix compression.

Table 4 Pore size distribution estimated by the combination of LTPA and MIP for coal samples from southern Junggar Basin

Sample No.	Pore content/volume (%)			
	V_1	V_2	V_3	V_4
NS-1	1.92	2.29	53.88	41.91
NS-2	4.57	5.41	34.22	55.81
MM2-4	0.79	1.65	22.22	75.34
TX-1	5.37	4.28	55.83	34.52
TX-2	11.12	8.80	57.00	23.07
XGG-1	15.55	7.96	30.71	45.77
KG-1-1	13.25	11.15	30.47	45.13
KG-1-2	15.24	9.64	49.35	25.77
KG-1-3	24.23	14.01	34.71	27.05
KG-1-4	18.21	10.29	39.89	31.61
KG-1-5	16.05	9.71	44.66	29.58
CXY-2	2.41	3.17	63.63	30.78

Notes: V_1, content of micropore (< 10 nm in diameter); V_2, content of transition pore (10–100 nm in diameter); V_3, content of mesopore (100–1000 nm in diameter); V_4, content of macropore (> 1000 nm in diameter).

5.2 Influencing factors of fractal dimensions (D_1 and D_2) and their effect on methane adsorption capacity

Many studies have confirmed that the methane adsorption capacity of coal is affected by various physical properties such as coal rank, macerals, moisture content, ash yield and pore structures (Yao et al., 2008; Fu et al., 2017a; Hou et al., 2017; Tao et al., 2018; Zhao et al., 2019). In this study, the D_1 and D_2 values have no obvious correlation with $R_{o,max}$ (Figs. 11(a) and 11(b)), which is closely related to the little physio-chemical changes of the coal during coalification. In the lower coalification stages, the hydroxyl and carboxyl functional groups in the coal have not begun to decrease, and there is little change in the aromaticity and condensation degree with the increase of coal rank (Yao et al., 2008; Fu et al., 2016a). Two samples (MM2-5 and MM2-7) with the D_1 values less than 2, which deviate from the natural fractal dimension, and one sample (MM2-1) with an abnormally high D_1 value, were excluded from the analysis. The D_1 and D_2 values have a polynomial correlation with moisture content (Figs. 11(c) and 11(d)). When the moisture content < 3.5%, the D_1 and D_2 values increase with increasing moisture contents. At this stage of low moisture content, affected by the liquid/gas surface tension, the adsorbate molecules may not be attached to the adsorbent surface, resulting in more complex coal pore surfaces and structures with increasing moisture content. When moisture content > 3.5%, the surface tension disappeared, and the filling by water increased the homogeneity of the coal pores, leading to the decrease of fractal dimensions (Yao et al., 2008). Previous study has proposed that volatile content decreases and fixed carbon content increases with the increase of coal rank (Fu et al., 2016a). As shown in Figs. 11(e) and 11(g), volatile content and fixed carbon content are negatively and positively correlated with D_1 respectively, indicating that D_1 increases with the increase of coal rank. D_1 is highly positively correlated with BET specific surface area, which further indicates that D_1 can be used to characterize pore surfaces (Fig. 11(i)). Coal with high D_1 values has more complex pore surfaces and a stronger methane adsorption capacity. Vitrinite provides more adsorption pores than inertinite (Faiz et al., 2007), which is beneficial to improve the adsorption capacity of the coal. There is a negative correlation between D_2 and vitrinite content, indicating that D_2 is closely related to pore structures, and the coal with lower D_2 has better gas adsorption capacity (Fig. 11(f)). The ash can infill the coal pores, which reduces the heterogeneity of adsorption pore structures, so that D_2 decreases with the increase of

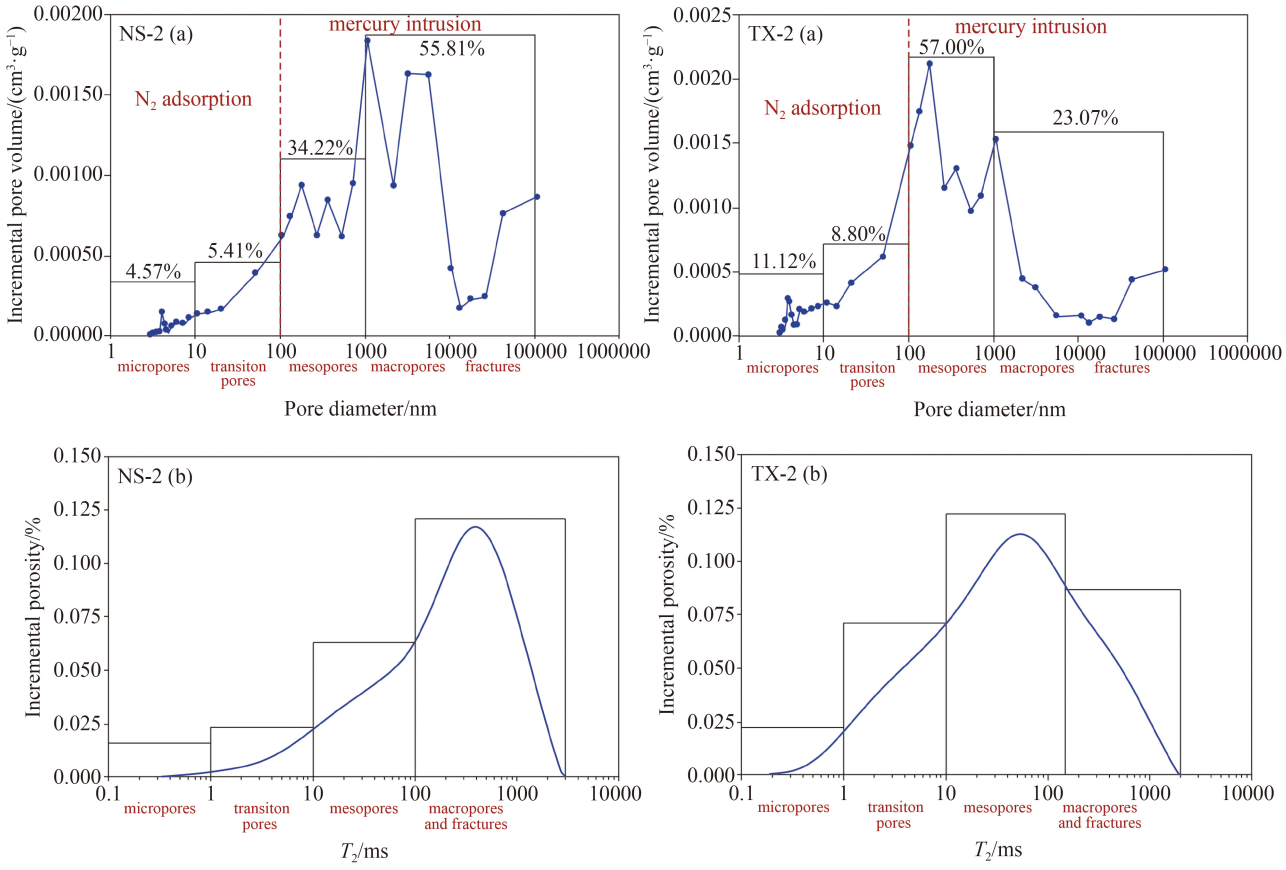

Fig. 10 Comparison of the pore size distribution by (a) LTNA and MIP joint analysis and (b) NMR relaxation.

ash yield (Fig. 11(h)). There is a strong negative correlation between D_2 and average pore size, with the correlation coefficient $R_2 = 0.9530$ (Fig. 11(j)), indicating that D_2 in low-rank coal increases with the increase of coal rank, and higher D_2 represents more complex pore structures and decreased methane adsorption capacity.

Langmuir volume (V_L) is often used as a direct indicator of the methane adsorption capacity of coal, and Langmuir pressure (P_L) can be used to indicate the difficulty of methane adsorption. As discussed above, D_1 and D_2 were used to characterize the pore surface and pore structure of adsorption pores related to methane adsorption, so the relationship between D_1 and D_2 and methane adsorption capacity was studied. There is a negative correlation between V_L and D_1 when $D_1 < 2.2$, and a positive correlation when $D_1 > 2.2$ (Fig. 12(a)); P_L and D_1 shows an opposite trend (Fig. 12(b)). The trend when $D_1 < 2.2$ may be caused by the special pore structures of Type C coal based on LTNA. When $D_1 > 2.2$, the pore specific surface area of coal increases with the increase of D_1, which leads to the enhancement of methane adsorption capacity. P_L decreases with the increase of D_1, indicating that methane is more easily adsorbed into coal with higher D_1. D_2 has a weak negative correlation with V_L and a weak positive correlation with P_L (Figs. 12(c) and 12(d)), which indicates that the lower D_2, then the stronger methane adsorption capacity. This is because with the increase of D_2, the vitrinite content and average pore sizes of coal decreases, the adsorption pores provided by vitrinite decreases, and the complexity of coal pore structures increases, resulting in the decrease of methane adsorption capacity of the coal. The results show that the methane adsorption capacity of coals with higher D_1 value and lower D_2 value is stronger. In addition, it was found that D_1 has a better fit with V_L and P_L than D_2, which is more suitable to characterize the adsorption capacity of low-rank coal.

5.3 Influencing factors of fractal dimensions (D_3 and D_4) and their effect on methane seepage capacity

To study the fractal features of the seepage pores and their influence on methane seepage capacity in low-rank coal, the relationships between fractal dimensions of the seepage pores (i.e., D_3 and D_4) and coal rank and composition, pore structure and seepage capacity were analyzed. Although deviating from the natural fractal dimension, D_3 and D_4 (> 3.4) still have obvious fractal features, which can be used to characterize the pore structures and seepage capacity of low-rank coals. There is a linear positive correlation between D_4 and $R_{o,max}$, which indicates that D_4 increases with the increase of coal rank, and higher D_4 represents more complex pore

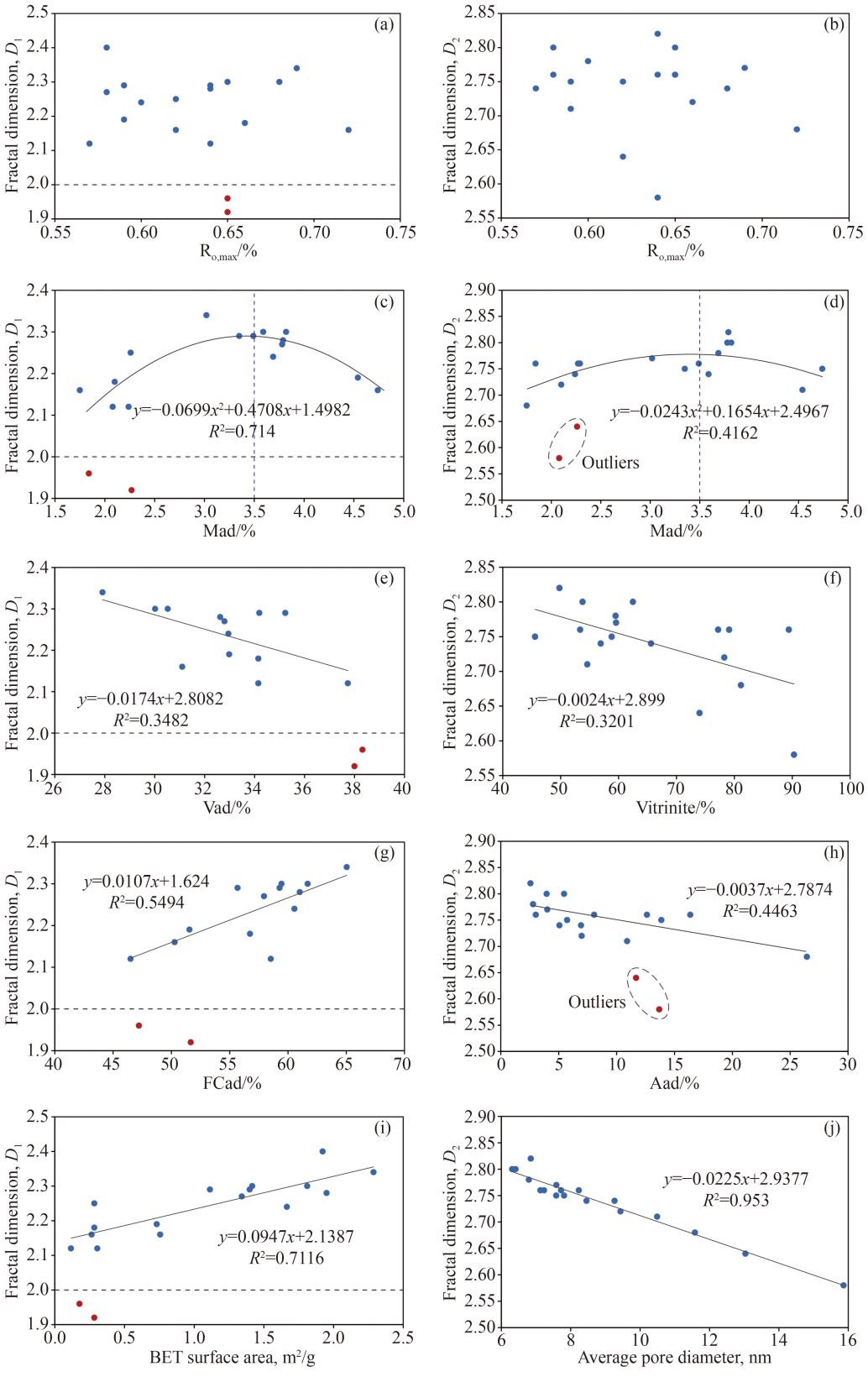

Fig. 11 Relationship between fractal dimensions D_1 and $R_{o,max}$, M_{ad}, V_{ad}, FC_{ad} and BET surface area (a, c, e, g, and i); and relationship between fractal dimensions D_2 and $R_{o,max}$, M_{ad}, vitrinite, A_{ad} and average pore diameter (b, d, f, h, and j).

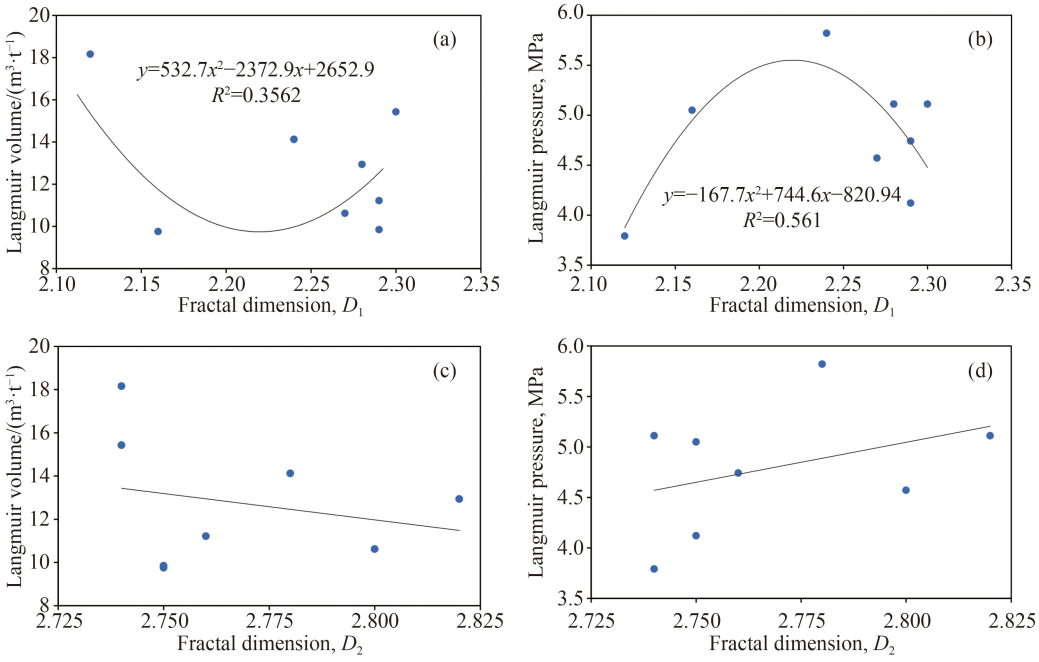

Fig. 12 Relationship between fractal dimensions D_1, D_2 and Langmuir volume, Langmuir pressure.

structures (Fig. 13(a)). However, D_3 presents a weak trend opposite to D_4, indicating that the lower the D_3, the more complex the pore structures of the coal (Fig. 13(b)). Compared with adsorption pores, the structure of seepage pores is more affected by the change of coal rank. As mentioned above, the volatile content of coal decreases with the increase of coal rank, which can also be proved by the obvious negative correlation between D_4 and volatile content (Fig. 13(d)). As shown in Fig. 13(c), there is no correlation between D_3 and volatile matter, which may be the result of the comprehensive control of fractal dimension D_3 by multiple factors such as coal rank, composition and pore structure (Yao et al., 2009). There was no significant correlation between D_3, D_4 and vitrinite contents, indicating that organic macerals had little effect on the pore structure of seepage pores (Figs. 13(e) and 13(f)). The main component of ash yield in coal is mineral, and the ash yield increases with the increase of mineral content (Hou et al., 2020a). D_3 is highly negatively correlated with ash yield, indicating that more mineral infilling can increase the heterogeneity and complexity of coal seepage pore structures (Fig. 13(g)). The negative correlation between D_4 and macropore content is related to the gradually enhanced physical compression of coal pores with the increase of coal rank (Fig. 13(h)), which is consistent with previous studies (Fu et al., 2017a; Zhao et al., 2019).

Porosity includes matrix porosity and cleat/fracture porosity, representing the volume fraction of pores in coal (Rodrigues and Lemos de Sousa, 2002; Cai et al., 2011). Permeability can be used to characterize the ability of gas migration in coal, and is an important index to evaluate gas production in coal (Pan et al., 2010). Many researchers have pointed out that the permeability decreases with the increase of fractal dimension of seepage pores (Yao et al., 2009; Zhao et al., 2019). However, as shown in Fig. 14, D_4 is significantly positively correlated with porosity and permeability, while D_3 shows a weak opposite trend, indicating that with the increase of coalification, the seepage capacity of low-rank coal is enhanced. This may be due to the relatively developed microfractures in the low-rank coal from the Xishanyao Formation increase the porosity and enhance the permeability of coal. In addition, compared with D_3, D_4 has a better fit with porosity and permeability, indicating that D_4 can better characterize the seepage capacity of low-rank coal than D_3.

6 Conclusions

1) The Xishanyao coal samples consist of three types of nitrogen adsorption/desorption curves (mainly Type B) and four types of mercury intrusion/extrusion curves (mainly Type A), indicating open pore morphology and good pore connectivity. Based on the combined analysis of LTNA and MIP, the coal pores are mainly mesopores, macropores and microfractures, while micropores and transition pores are poorly developed, which is in good agreement with the SEM observation and PSD evaluated by NMR. The results show that the pore structure of the Xishanyao low-rank coal is beneficial to CBM seepage, but not conducive to CBM adsorption.

2) D_1 and D_2 can be used to characterize the pore surface and structure of adsorption pores respectively. D_1 and D_2 increase with increasing coal rank due to the enhanced complexity of pore surfaces and structures;

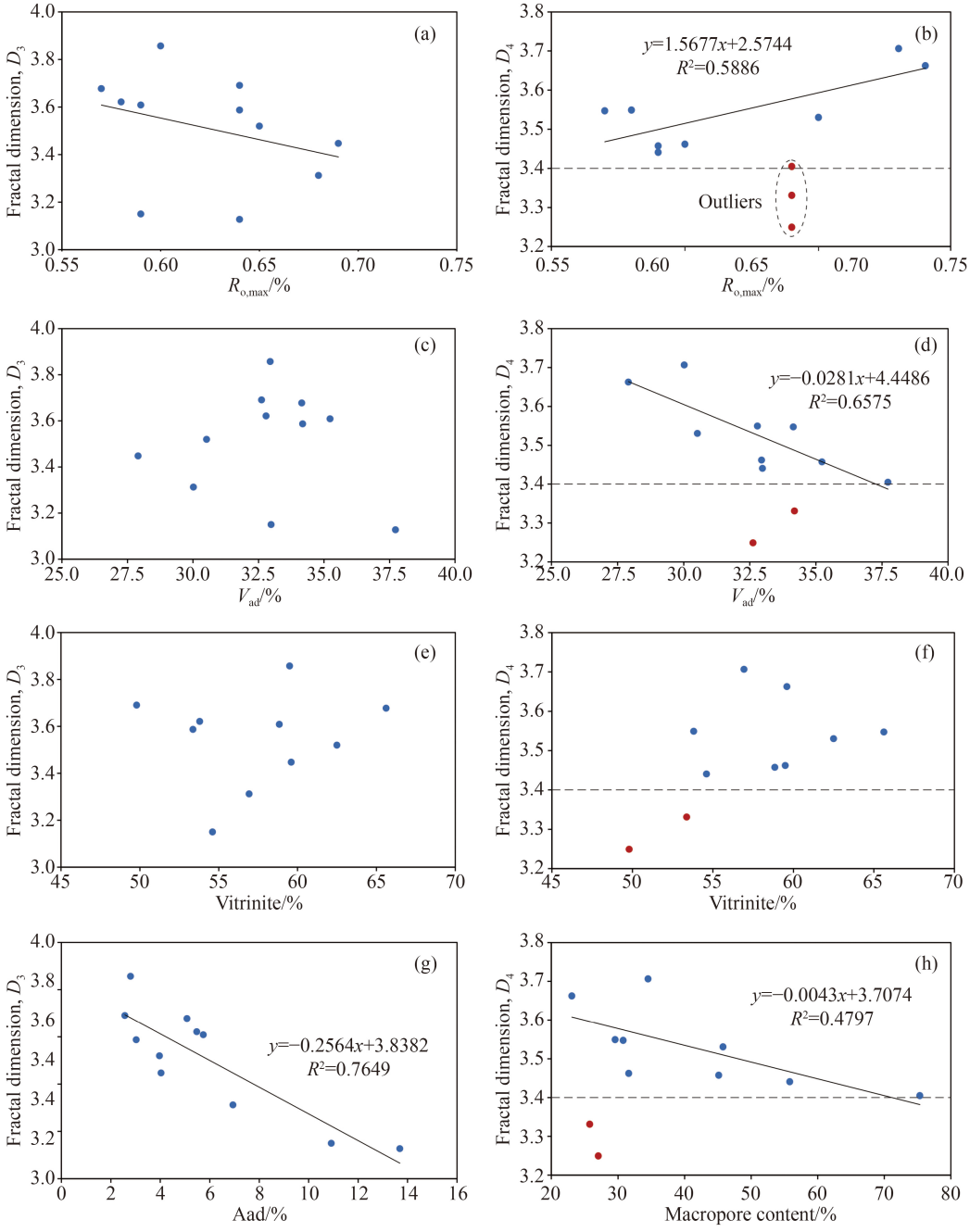

Fig. 13 Relationship between fractal dimension D_3 and $R_{o,max}$, V_{ad}, vitrinite and A_{ad} (a, c, e, and g); and relationship between fractal dimension D_4 and $R_{o,max}$, V_{ad}, vitrinite and macropore content (b, d, f, and h).

Both D_3 and D_4 can represent the pore structure of seepage pores. D_3 decreases with the increase of coal rank, while D_4 shows an opposite trend, which may be related to the deviation from the natural fractal dimension. Compared with adsorption pores, the structure of seepage pores is more affected by the change of coal rank. In addition, the macerals can affect the fractal dimensions of adsorption pores but not the seepage pores.

3) D_1 can better characterize the methane adsorption capacity than D_2. When $D_1 > 2.2$, D_1 is positively correlated with V_L and negatively correlated with P_L, while D_2 shows a weak opposite trend. The coals with higher D_1 and lower D_2 have higher V_L, which indicates that the coals with more complex pore surfaces and simpler pore structures have stronger methane adsorption capacity; D_4 can better characterize methane seepage capacity than D_3. The porosity and permeability of coals increases with the increase of D_4, while D_3 presents the opposite trend, which may be related to the good development of microfractures in the Xishanyao coal. The well-developed fracture system enhances the seepage capacity of the coal.

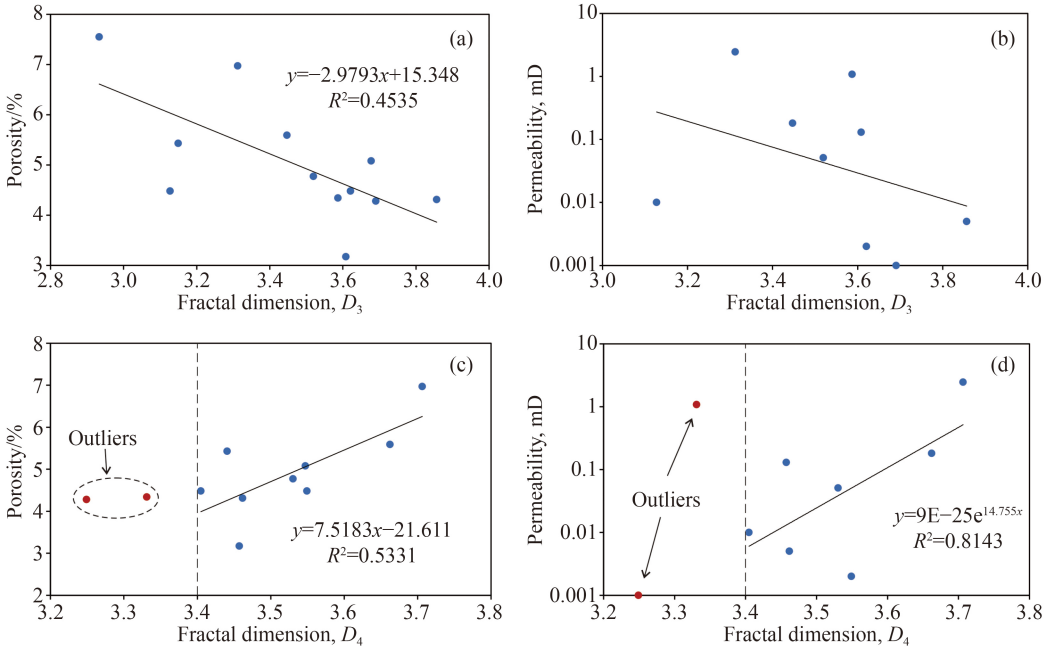

Fig. 14 Relationship between fractal dimension D_3 and porosity (a) and permeability (b) and relationship between fractal dimension D_4 and porosity (c) and permeability (d).

Acknowledgements This study was supported by the China Geological Survey Scientific Research Project (Nos. DD20160204-3 and DD20160204-YQ17W01), the Yue Qi Scholar Project of China University of Mining and Technology (Beijing) and Fundamental Research Funds for the Central University (No. 2022YJSDC05). The authors are grateful to the anonymous reviewers for their careful reviews and constructive comments.

References

Ashraf A R, Sun Y, Sun G, Uhl D, Mosbrugger V, Li J, Herrmann M (2010). Triassic and Jurassic palaeoclimate development in the Junggar Basin, Xinjiang, northwest China—a review and additional lithological data. Palaeobiodivers Palaeoenviron, 90(3): 187–201

Ayers W B Jr (2002). Coalbed gas systems, resources, and production and a review of contrasting cases from the San Juan and Powder River basins. AAPG Bull, 86(11): 1853–1890

Barrett E P, Joyner L G, Halenda P P (1951). The determination of pore volume and area distributions in porous substances. I. Computations from nitrogen isotherms. J Am Chem Soc, 73(1): 373–380

Brunauer S, Emmett P H, Teller E (1938). Adsorption of gases in multimolecular layers. J Am Chem Soc, 60(2): 309–319

Cai Y D, Liu D M, Yao Y B, Li J Q, Qiu Y K (2011). Geological controls on prediction of coalbed methane of No. 3 coal seam in Southern Qinshui Basin, north China. Int J Coal Geol, 88(2−3): 101−112

Cai Y D, Liu D M, Pan Z J, Yao Y B, Li J Q, Qiu Y K (2013). Pore structure and its impact on CH_4 adsorption capacity and flow capability of bituminous and subbituminous coals from northeast China. Fuel, 103: 258–268

Chen B, Arakawa Y (2005). Elemental and Nd-Sr isotopic geochemistry of granitoids from the West Junggar foldbelt (NW China), with implications for Phanerozoic continental growth. Geochim Cosmochim Acta, 69(5): 1307–1320

Cheng A G, Cao D Y, Yuan T X (2016). China Occurrence Regularity of Coal Resources and Resource Evaluation. Beijing: Science Press (in Chinese)

Faiz M, Saghafi A, Sherwood N, Wang I (2007). The influence of petrological properties and burial history on coal seam methane reservoir characterisation, Sydney Basin, Australia. Int J Coal Geol, 70(1−3): 193–208

Fang Y N, Wu C D, Wang Y Z, Wang L X, Guo Z J, Hu H W (2016). Stratigraphic and sedimentary characteristics of the upper jurassic-lower cretaceous strata in the Junggar basin, central Asia: tectonic and climate implications. J Asian Earth Sci, 129: 294–308

Flores R M, Rice C A, Stricker G D, Warden A, Ellis M S (2008). Methanogenic pathways of coal-bed gas in the Powder River Basin, United States: the geologic factor. Int J Coal Geol, 76(1-2): 52–75

Friesen W I, Mikula R J (1987). Fractal dimensions of coal particles. J Colloid Interface Sci, 120(1): 263–271

Fu H J, Tang D Z, Xu H, Tao S, Xu T, Chen B L, Yin Z Y (2016a). Abrupt changes in reservoir properties of low-rank coal and Its control factors for methane adsorbability. Energy Fuels, 30(3): 2084–2094

Fu H J, Tang D Z, Xu H, Xu T, Chen B L, Hu P, Yin Z, Wu P, He G (2016b). Geological characteristics and CBM exploration potential evaluation : a case study in the middle of the southern Junggar Basin, NW China. J Nat Gas Sci Eng, 30: 557–570

Fu H J, Tang D Z, Xu T, Xu H, Tao S, Li S, Yin Z Y, Chen B L, Zhang C, Wang L (2017a). Characteristics of pore structure and fractal dimension of low-rank coal : a case study of Lower Jurassic Xishanyao coal in the southern Junggar Basin, NW China. Fuel, 193: 254–264

Fu H J, Tang D Z, Xu T, Xu H, Tao S, Zhao J L, Chen B, Yin Z

(2017b). Preliminary research on CBM enrichment models of low-rank coal and its geological controls : a case study in the middle of the southern Junggar Basin. Mar Pet Geol, 83: 97–110

Fu X H, Qin Y, Xue X Q, Li G Z, Wang W F (2001). Research on fractals of pore and fracture-structure of coal reservoirs. J China Univ Min Technol, 03: 11−14 (in Chinese)

Giesche H (2006). Mercury porosimetry: a general (practical) overview. Part Part Syst Charact, 23(1): 9–19

Hassan J (2012). Pore size distribution calculation from ^{1}H NMR signal and N_2 adsorption-desorption techniques. Phys B Condens Matter, 407(18): 3797–3801

Heriawan M N, Koike K (2015). Coal quality related to microfractures identified by CT image analysis. Int J Coal Geol, 140: 97–110

Hodot B B (1966). Outburst of Coal and Coalbed Gas. Beijing: China Industry Press: 23–35

Hou H H, Shao L Y, Li Y H, Li Z, Wang S, Zhang W L, Wang X T (2017). Influence of coal petrology on methane adsorption capacity of the Middle Jurassic coal in the Yuqia Coalfield, northern Qaidam Basin, China. J Petrol Sci Eng, 149: 218–227

Hou H H, Shao L Y, Li Y H, Li Z, Zhang W L, Wen H J (2018). The pore structure and fractal characteristics of shales with low thermal maturity from the Yuqia Coalfield, northern Qaidam Basin, northwestern China. Front Earth Sci, 12(1): 148–159

Hou H H, Shao L Y, Tang Y, Zhao S, Yuan Y, Li Y N, Mu G Y, Zhou Y, Liang G D, Zhang J Q (2020a). Quantitative characterization of low-rank coal reservoirs in the southern Junggar Basin, NW China: implications for pore structure evolution around the first coalification jump. Mar Pet Geol, 113: 104165

Hou H H, Shao L Y, Tang Y, Li Y N, Liang G D, Xin Y L, Zhang J Q (2020b). Coal seam correlation in terrestrial basins by sequence stratigraphy and its implications for palaeoclimate and palaeoenvironment evolution. J Earth Sci

Hou H H, Liang G D, Shao L Y, Tang Y, Mu G Y (2021). Coalbed methane enrichment model of low-rank coals in multi-coals superimposed regions: a case study in the middle section of southern Junggar Basin. Front Earth Sci, 15(2): 256–271

Jiang J Y, Zhang Q, Cheng Y P, Jin K, Zhao W, Guo H J (2016). Influence of thermal metamorphism on CBM reservoir characteristics of low-rank bituminous coal. J Nat Gas Sci Eng, 36: 916–930

Li A, Ding W L, He J H, Dai P, Yin S, Xie F (2016a). Investigation of pore structure and fractal characteristics of organic-rich shale reservoirs: a case study of Lower Cambrian Qiongzhusi formation in Malong block of eastern Yunnan Province, south China. Mar Pet Geol, 70: 46–57

Li Y, Zhang C, Tang D Z, Gan Q, Niu X L, Wang K, Shen R Y (2017). Coal pore size distributions controlled by the coalification process: an experimental study of coals from the Junggar, Ordos and Qinshui basins in China. Fuel, 206: 352–363

Li Y, Cao D Y, Wei Y C, Wang A M, Zhang Q, Wu P (2016b). Middle to low rank coalbed methane accumulation and reservoiring in the southern margin of Junggar Basin. Acta Petrol Sin, 37(12): 1472−1482 (in Chinese)

Li Y N, Shao L Y, Hou H H, Tang Y, Yuan Y, Zhang J Q, Shang X X, Lu J (2018). Sequence stratigraphy, palaeogeography, and coal accumulation of the fluvio-lacustrine Middle Jurassic Xishanyao Formation in central segment of southern Junggar Basin, NW China. Int J Coal Geol, 192: 14–38

Ma D L, He D F, Li D, Tang J Y, Liu Z (2015). Kinematics of syn-tectonic unconformities and implications for the tectonic evolution of the Hala'alat Mountains at the northwestern margin of the Junggar Basin, Central Asian Orogenic Belt. Geosci Front, 6(2): 247–264

Mahamud M M (2006). Textural characterization of active carbons using fractal analysis. Fuel Process Technol, 87(10): 907–917

Mahamud M M, Novo M F (2008). The use of fractal analysis in the textural characterization of coals. Fuel, 87(2): 222–231

Mandelbrot B B (1975). Stochastic models for the Earth's relief, the shape and the fractal dimension of the coastlines, and the number-area rule for islands. Proc Natl Acad Sci, 72(10): 3825–3828

Mendhe V A, Bannerjee M, Varma A K, Kamble A D, Mishra S, Singh B D (2017). Fractal and pore dispositions of coal seams with significance to coalbed methane plays of East Bokaro, Jharkhand, India. J Nat Gas Sci Eng, 38: 412–433

Mou P W, Pan J N, Niu Q H, Wang Z Z, Li Y B, Song D Y (2021). Coal pores: methods, types, and characteristics. Energy Fuels, 35(9): 7467–7484

Neimark A V (1990). Determination of surface fractal dimension from the results of an adsorption experiment. Russ J Phys Chem, 64: 1397–1403

Nie B S, Liu X F, Yang L L, Meng J Q, Li X C (2015). Pore structure characterization of different rank coals using gas adsorption and scanning electron microscopy. Fuel, 158: 908–917

Pan J N, Niu Q H, Wang K, Shi X H, Li M (2016). The closed pores of tectonically deformed coal studied by small-angle X-ray scattering and liquid nitrogen adsorption. Microporous Mesoporous Mater, 224: 245–252

Pan Z J, Connell L D, Camilleri M (2010). Laboratory characterisation of coal reservoir permeability for primary and enhanced coalbed methane recovery. Int J Coal Geol, 82(3−4): 252–261

Pfeifer P, Avnir D (1983). Chemistry in noninteger dimensions between two and three. I. Fractal theory of heterogeneous surfaces. J Chem Phys, 79(7): 3558–3565

Pfeifer P, Wu Y J, Cole M W, Krim J (1989). Multilayer adsorption on a fractally rough surface. Phys Rev Lett, 62(17): 1997–2000

Qin Y, Moore T A, Shen J, Yang Z B, Shen Y L, Wang G (2018). Resources and geology of coalbed methane in China : a review. Int Geol Rev, 60(5−6): 777–812

Rodrigues C F, Lemos de Sousa M J (2002). The measurement of coal porosity with different gases. Int J Coal Geol, 48(3−4): 245–251

Shao L Y, Zhang P F, Hilton J, Gayer R, Wang Y B, Zhao C Y, Luo Z (2003). Paleoenvironments and paleogeography of the Lower and lower Middle Jurassic coal measures in the Turpan-Hami oil-prone coal basin northwestern China. Am Assoc Pet Geol Bull, 87(2): 335–355

Shao L Y, Hou H H, Tang Y, Lu J, Qiu H J, Wang X T, Zhang J Q (2015). Selection of strategic replacement areas for CBM exploration and development in China. Nat Gas Ind B, 2(2−3): 211–221

Shen P, Pan H D, Shen Y C, Yan Y H, Zhong S H (2015). Main

deposit styles and associated tectonics of the West Junggar region, NW China. Geosci Front, 6(2): 175–190

Sun F J, Li W Z, Sun Q P, Sun B, Tian W G, Chen Y J, Chen Z H (2017). Low-rank coalbed methane exploration in Jiergalangtu Sag, Erlian Basin. Acta Petrol Sin, 38(5): 485−492 (in Chinese)

Sun X X, Yao Y B, Liu D M, Zhou Y F (2018). Investigations of CO_2-water wettability of coal: NMR relaxation method. Int J Coal Geol, 188: 38–50

Tang J Y, He D F, Li D, Ma D L (2015). Large-scale thrusting at the northern Junggar Basin since Cretaceous and its implications for the rejuvenation of the Central Asian Orogenic Belt. Geoscience Frontiers, 6(2): 227–246

Tao S, Tang D Z, Xu H, Gao L J, Fang Y (2014). Factors controlling high-yield coalbed methane vertical wells in the Fanzhuang Block, southern Qinshui Basin. Int J Coal Geol, 134−135: 38−45

Tao S, Chen S D, Tang D Z, Zhao X, Xu H, Li S (2018). Material composition, pore structure and adsorption capacity of low-rank coals around the first coalification jump: a case of eastern Junggar Basin, China. Fuel, 211: 804–815

Thommes M, Kaneko K, Neimark A V, Olivier J P, Rodriguez-reinoso F, Rouquerol J, Sing K S W (2015). Physisorption of gases, with special reference to the evaluation of surface area and pore size distribution (IUPAC Technical Report). Pure Appl Chem, 87(9−10): 1051–1069

Wang F, Cheng Y P, Lu S Q, Jin K, Zhao W (2014). Influence of coalification on the pore characteristics of middle–high rank coal. Energy Fuels, 28(9): 5729–5736

Wang M, Xue H T, Tian S S, Wilkins R W T, Wang Z W (2015). Fractal characteristics of Upper Cretaceous lacustrine shale from the Songliao Basin, NE China. Mar Pet Geol, 67: 144–153

Wang X L, Pan J N, Wang K, Ge T Y, Wei J, Wu W (2020). Characterizing the shape, size, and distribution heterogeneity of pore-fractures in high rank coal based on X-Ray CT image analysis and mercury intrusion porosimetry. Fuel, 282: 118754

Yao Y B, Liu D M, Tang D Z, Tang S H, Huang W H (2008). Fractal characterization of adsorption-pores of coals from North China : an investigation on CH_4 adsorption capacity of coals. Int J Coal Geol, 73(1): 27–42

Yao Y B, Liu D M, Tang D Z, Tang S H, Huang W H, Liu Z H, Che Y (2009). Fractal characterization of seepage-pores of coals from China: an investigation on permeability of coals. Comput Geosci, 35(6): 1159–1166

Yao Y B, Liu D M, Che Y, Tang D Z, Tang S H, Huang W H (2010). Petrophysical characterization of coals by low-field nuclear magnetic resonance (NMR). Fuel, 89(7): 1371–1380

Yao Y B, Liu D M (2012). Comparison of low-field NMR and mercury intrusion porosimetry in characterizing pore size distributions of coals. Fuel, 95: 152–158

Zhang S H, Tang S H, Tang D Z, Huang W H, Pan Z J (2014). Determining fractal dimensions of coal pores by FHH model: problems and effects. J Nat Gas Sci Eng, 21: 929–939

Zhao J L, Tang D Z, Qin Y, Xu H (2019). Fractal characterization of pore structure for coal macrolithotypes in the Hancheng area, southeastern Ordos Basin, China. J Petrol Sci Eng, 178: 666–677

Zhou S D, Liu D M, Cai Y D, Karpyn Z, Yao Y B (2018). Petrographic controls on pore and fissure characteristics of coals from the southern Junggar Coalfield, northwest China. Energies, 11(6): 1556

Zhu J F, Liu J Z, Yang Y M, Cheng J, Zhou J H, Cen K F (2016). Fractal characteristics of pore structures in 13 coal specimens: relationship among fractal dimension, pore structure parameter, and slurry ability of coal. Fuel Process Technol, 149: 256–267